www.acsmaterialsletters.org

Linker Aromaticity Reduces Band Dispersion in 2D Conductive Metal-Organic Frameworks

Monique C. Demuth and Christopher H. Hendon*



Downloaded via UNIV OF OREGON on April 12, 2023 at 15:33:55 (UTC). See https://pubs.acs.org/sharingguidelines for options on how to legitimately share published articles.

Cite This: ACS Materials Lett. 2023, 5, 1476-1480



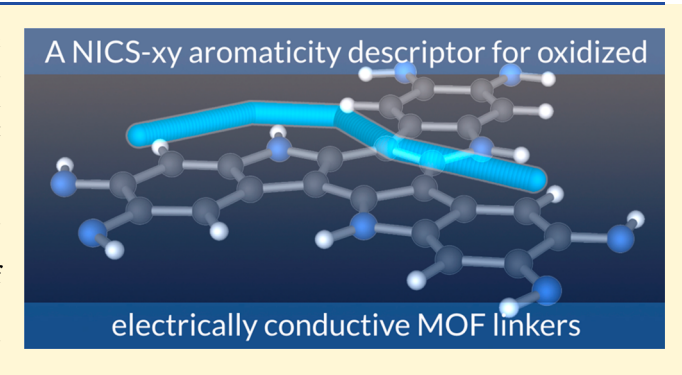
ACCESS

Metrics & More

Article Recommendations

Supporting Information

ABSTRACT: All 2D electrically conductive metal-organic frameworks (MOFs) are constructed from hexasubstituted aromatics that oxidize during self-assembly. Since electrical conduction is thought to occur through the ligand π -system, but aromaticity itself results in stabilized π -electrons, the delocalization of ligand wavefunctions should be inversely related to the ligand π -stability. That is, aromatic π -electrons should prefer to localize on a single linker rather than delocalize to form a curved band in the MOF. Here, we use a combination of NICS-xy scans and bulk electronic band structure calculations to show that the extent of residual aromaticity in the oxidized linker is a good predictor for electronic localization in the



resultant MOF. Thus, ligands that feature antiaromatic π -systems in the oxidation state found within the MOF should yield increased band curvature, a target parameter that affects charge mobility in high performing electrical conductors.

he discovery of high-surface-area electrical conductors is critical for developing electrodes for capacitive energy storage. 1,2 Toward this goal, the realization of electrically conductive MOFs^{3,4} has spurred the development of novel porous conductors featuring 2D- and 3D-connected scaffolds with conductivities exceeding 100 S/cm, making them a viable manifold for real-world energy storage devices.⁶⁻⁸ The peak performing materials are 2D-connected kagome lattices⁹ composed of divalent metals^{10–12} paired with a hexasubsituted triphenylene linker (e.g., hexaiminotriphenylene (HITP)¹³ and hexahydroxytriphenyelene (HHTP)¹⁴). In those cases, both crystallinity and doping mechanisms are areas of active development but there are also outstanding knowledge gaps in how the ligand composition affects the bulk material properties.

In square-planar Ni²⁺ and Cu²⁺ molecular complexes, 15-17 the degree of ligand redox noninnocence depends on the energetics and geometry of the ligand orbitals, where increased covalency results in large molecular orbital splitting. Related MOFs¹⁸ are formed through the general assembly shown in Scheme 1. There, the ligand is both deprotonated and oxidized, and the MOFs are obtained from a goldilocks scenario where the linker is oxidized to achieve both charge neutrality and covalency. Hence, a central focus of ligand development is the control of electronic induction in the interior of the ring system, which should be an opposing driving force to increasing band dispersion (one property of bulk electronic delocalization). Herein, we show that some

Scheme 1. Kagome MOFs Obtain Charge Neutrality by Deprotonation and Oxidation of the Linker, Each Which Can Be Drawn in Many Resonance Forms, Including As Either a Quartet or Doublet

$$H_2N$$
 NH_2
 NH_2
 NH_2
 $-6H^+, -3e^ NH_2$
 NH_2
 NH_2

Received: February 4, 2023 Accepted: April 10, 2023



degree of aromaticity persists in the oxidized linkers found in the 2D conductive MOFs and is directly related to the bandwidth of MOFs made therefrom. From xy-plane nucleus-independent chemical shift (NICS-xy) scans paired with periodic DFT computations of 2D Ni-based MOFs (Cu-analogues are presented in the Supporting Information), we posit that the propensity for π -electrons to aromatize opposes electronic delocalization in the crystalline MOF (i.e., band curvature and resultant charge mobility 1, in effect yielding less favorable conduction pathways.

Given the family of 2D conductors are prone to stacking faults (2D sheet slipping), the extent of out-of-plane dispersion depends heavily on noncovalent orientation.²² While bulk electronic properties will naturally depend on the van der Waals stacking, the monolayer provides critical insights into "through-bond" electronic interactions.²³ Some of the 2D materials are predicted to be narrow gap semiconductors in the monolayer but have bulk metallicity (as in $Ni_3(HITP)_2$, HITP = hexaiminotriphenylene). ^{24–27} In those cases, the monolayer calculations serve a lower estimate of the most conductive crystallographic direction. In other cases, the monolayer may be metallic (as in Ni₃(HIB)₂, HIB = hexaiminobenzene²⁸ and other hexasubstituted benzenes²⁹), in which case the monolayer may possess the most conductive crystallographic plane. Regardless, by examining a systematically altered family of experimentally tractable 2D MOFs we can study the ligand's π -system and its impact on predicted band curvature, a property that affects bulk conductivity.

To do so, we first construct a small library of plausible linkers used in the formation of 2D MOFs, Figure 1a. These systems were selected as they canvas both known linkers, and synthetically plausible structures with appropriate 3-connected geometries and have been used in other conductive materials. $^{30-34}$ In order to achieve charge neutrality in a bulk MOF of nominal stoichiometry metal₃linker₂, the metal is 2+ (e.g., Ni²+, Cu²+) and the linker is 3–. This is achieved by six deprotonations and three oxidation events, yielding a radical (either a quartet or doublet depending on the propensity for two radicals to pair, Scheme 1). These exocyclic compounds, shown as quartets in Figure 1a, have a nominal $\rm C_3$ rotational axis, and our DFT calculations suggest that the doublet is more favorable than the depicted quartet.

NICS-xy scans can then be used to probe the degree of aromatic/antiaromatic character and π delocalization by sampling the extent of deshielding of a fictitious atom positioned 1.7 Å above the ring system. 35,36 While the NICS-xy scan is not conventionally used for exocyclic compounds it is instructive in this case, as there are internal ring systems that may have aromatic character depending on the locality and pairing of the radicals, per Scheme 1. These scans are presented in Figure 1b, following a sampling path presented in Figure 1c. HIB is a nonaromatic compound and the NICS scan results in a +350 ppm shift, Figure S1. Perhaps this could be interpreted as being highly antiaromatic, although NICS-xy scans are less applicable to systems that are neither aromatic or antiaromatic; a three electron oxidation of HIB satisfies neither 4n or 4n+2 π electrons. The other linkers, HHTP, HITP, HITT, HHTT, and HIIB exhibit an increasing degree of aromaticity, attributed to a progressively more delocalized π -system across more C/N/O centers (an example of a S-substituted linker is presented in Figure S1). This aligns with our chemical intuition, as the larger linker maintains more aromatic character as more π -electrons need to be removed to

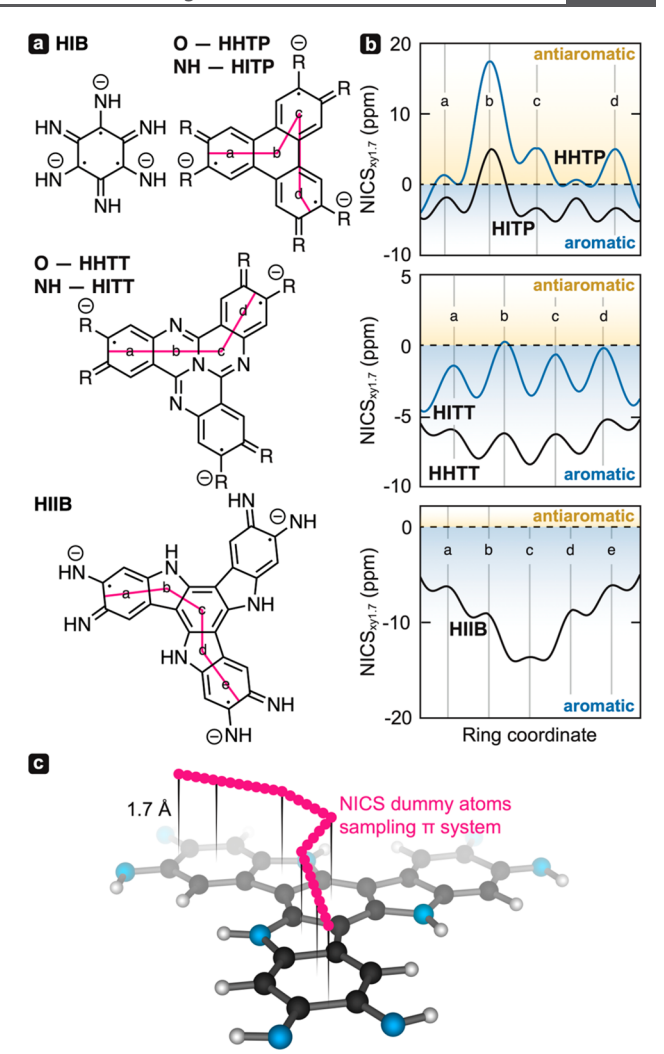


Figure 1. Ligands and their associated NICS-xy scans examined in this study. (a) The ligands are depicted in their formal oxidation and charge state as they appear in the charge neutral MOF of nominal stoichiometry M_3L_2 . Hexaiminobenzene (HIB), the hydroxy and imino triphenylenes (HHTP and HITP, respectively), and the hexahydroxy tetraazanaphthotetraphene (HHTT) have been synthesized with both Ni^{2+} and Cu^{2+} . The imino functionalized tetraazanaphthotetraphene (HITT) and the indolo-benzene (HIIB) were included as logical derivatives. (b) The associated NICS-xy scans probed at (c) 1.7 Å for the doublet ligands. Aromatic and antiaromatic signatures are negative (blue) and positive (yellow) chemical shifts, respectively. The NICS-xy paths are labeled a-e, and the path is depicted by the pink line.

fully dearomatize it. A similar conclusion can also be gleaned from examination of the spin density, Figure S2.

In fact, the spin density was used to instruct the NICS-xy sampling paths. In the case of HITP and HHTP, the conventional pathway would be to sample a-b-c (Figure 1a), but we wanted to demonstrate that the doublet results in electronic asymmetry where the a center is nominally less antiaromatic than the c and d centers, which are indistinguishable. The asymmetry was also visible in the spin density. For the other linkers, we simply followed a path that traversed the two dissimilar chemical environments. Both HITT and HHTT show slightly more aromatic character. One can imagine that this is achieved by ionizing N-bound electrons, rather than C-bound neighbors. Finally, the HIIB linker appears to maintain

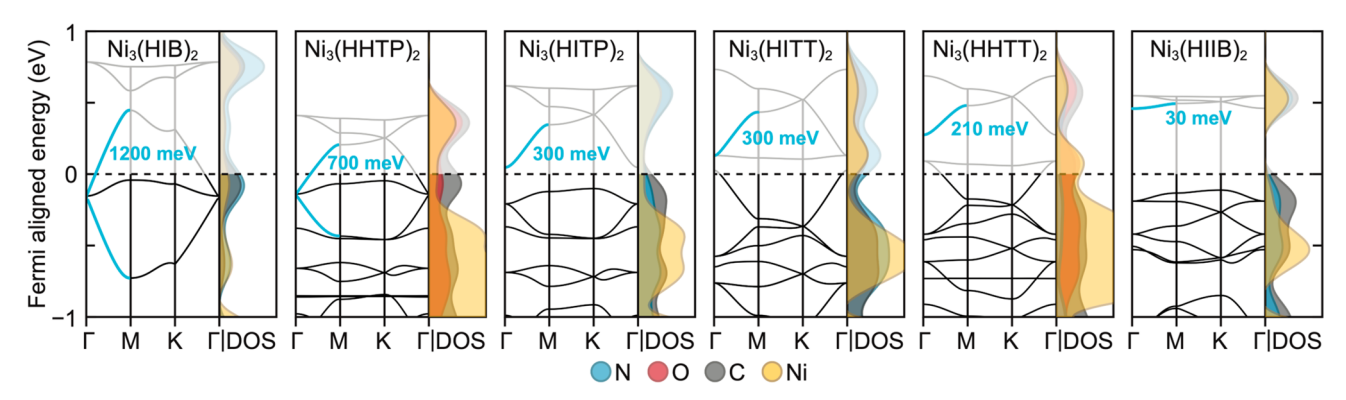


Figure 2. Electronic band structures and density of states of monolayer two-dimensional MOFs constructed from the six linkers. The lowest energy ligand-centered conduction band and its width are emphasized in blue.

aromatic character despite being oxidized. This result highlights that the N p-electrons play a supporting role in maintaining aromaticity. Together, these molecular calculations suggest larger π -systems can mitigate the effect of oxidation, particularly those with heteroatoms. With this in mind, we would then expect that more stabilized electrons should result in diminished band dispersion (delocalization) in materials made therefrom.

To probe this hypothesis, we next computed the electronic band structure and accompanying density of states (DOS) for the monolayer 2D Ni²⁺-MOFs, Figure 2 (Cu²⁺-MOFs are presented in Figure S3). There are some common features in the electronic band structures, including the emergence of relatively flat bands associated with metal-centered DOS. This effect is particularly pronounced in the Cu²⁺ systems, which inherently have a half-populated Cu $d_{x^2-y^2}$ orbital.

To simplify the analysis, we will focus on the Ni²⁺ materials presented in Figure 2, but note that the same concepts apply to the Cu systems. We selected the first conduction band with primarily linker character (these bands are highlighted in blue). Including band unfolding, the bandwidths (dispersion) are labeled on the figure and decrease with increasing aromatic character of the linker. That is, the HIIB is predicted to have the widest electronic band gap (~500 meV), and the smallest conduction band dispersion (30 meV) of the computed MOFs. Ni₃HIB₂ shows the largest band dispersion of any of the 2D MOFs, likely due to the highly unstable "antiaromatic" character of the free linker, Figure S1.

Perhaps most interesting are the features that appear in comparison of the HITP- and HHTP-based MOFs. While the Ni_3 HITP2 material is the experimental champion conductor, Ni_3 HHTP2 features a folded band at Γ , effectively doubling the bandwidth, and resulting in metallicity. These data suggest that HHTP-based materials should offer some upside relative to HITP-analogues. Of course, band curvature is only one factor in determining bulk conductivity, with the other operative parameters (charge carrier concentration and charge carrier identity) playing a critical role. To this end, the key challenge in these materials remains the control of the Fermi level, which in turn depends on the defect contributions in the material and is an area of ongoing interest.

Through a combination of NICS-xy scans and bulk electronic band structure calculations of monolayer Ni-based MOFs, we have concisely demonstrated that there is a direct relationship between material band dispersion and degree of (anti)aromaticity of the linker, computed in the same protonation and charge state as is found in the MOF. Looking

forward, these results indicate that the formation MOFs with highly curved electronic bands can be accessed by designing linkers that do not have a propensity to aromatize. There is hence a tension targeting linkages that are synthetically tractable but reactive enough to form exotic, relatively destabilized radicals. The results also highlight the critical role of controlling the Fermi level through defect engineering and metal selection. Finally, these data further point to a fundamental challenge in conductive MOF development—larger ligands increase accessible porosity to the detriment of band curvature in the resultant MOF.

COMPUTATIONAL METHOD

Molecular calculations were performed in Gaussian09,³⁷ using the B3LYP hybrid functional with a triple- ζ basis, 6-311+G*. NICS-xy scans were generated using Aroma, a free software package that creates the sampling paths and parses the shielding information. Periodic boundary calculations were performed within the Kohn–Sham DFT framework as implemented in Vienna *ab initio* simulation package (VASP 5.4.4).³⁸ Beginning with crystallographic unit cells of Ni₃(HIB)₂, the lattice parameters and atomic positions were equilibrated using the PBEsol functional,³⁹ with a Γ-centered 4 × 4 × 2 k-mesh and 500 eV planewave cutoff. Convergence was reached at 0.025 eV/atom. HSEsol⁴⁰ was then used to recover the electronic band structures and density of states. Other materials were manually constructed through ligand substitution.

ASSOCIATED CONTENT

Supporting Information

The Supporting Information is available free of charge at https://pubs.acs.org/doi/10.1021/acsmaterialslett.3c00122.

NICS-xy scans on the hexaiminobenzene and hexathiotriphenylene, associated electronic spin density isosurfaces for all ligands, and the 2D electronic band structures of the Ni- and Cu-containing MOFs (PDF)

AUTHOR INFORMATION

Corresponding Author

Christopher H. Hendon — Department of Chemistry and Biochemistry, University of Oregon, Eugene, Oregon 97403, United States; orcid.org/0000-0002-7132-768X; Email: chendon@uoregon.edu

Author

Monique C. Demuth – Department of Chemistry and Biochemistry, University of Oregon, Eugene, Oregon 97403, United States

Complete contact information is available at: https://pubs.acs.org/10.1021/acsmaterialslett.3c00122

Notes

The authors declare no competing financial interest.

ACKNOWLEDGMENTS

This work is supported by the National Science Foundation under Grant DMR-1956403, and the Research Corporation for Science Advancement (Cottrell Scholar Program) for non-tenured faculty. Computations were performed using the High-Performance Computing Cluster at the University of Oregon (Talapas), the Extreme Science and Engineering Discovery Environment (XSEDE), which is supported by National Science Foundation Grant ACI-1548562, and the Portland State University machine, Coeus, which is supported by the NSF (DMS1624776). The authors are grateful to Dr. G. Warren and Prof. M. Haley for their valuable insights into NICS-xy scans and how to interpret them and to Prof. J.-H. Dou for his thoughts in 2017 on useful linker compositions.

REFERENCES

- (1) Winter, M.; Brodd, R. J. What Are Batteries, Fuel Cells, and Supercapacitors? *Chem. Rev.* **2004**, *104*, 4245–4270.
- (2) Simon, P.; Gogotsi, Y. Materials for Electrochemical Capacitors. *Nat. Mater.* **2008**, *7*, 845–854.
- (3) Xie, L. S.; Skorupskii, G.; Dincă, M. Electrically Conductive Metal-Organic Frameworks. *Chem. Rev.* **2020**, *120*, 8536–8580.
- (4) Li, P.; Wang, B. Recent Development and Application of Conductive MOFs. *Isr. J. Chem.* **2018**, *58*, 1010–1018.
- (5) Day, R. W.; Bediako, D. K.; Rezaee, M.; Parent, L. R.; Skorupskii, G.; Arguilla, M. Q.; Hendon, C. H.; Stassen, I.; Gianneschi, N. C.; Kim, P.; Dincă, M. Single Crystals of Electrically Conductive Two-Dimensional Metal-Organic Frameworks: Structural and Electrical Transport Properties. ACS Cent. Sci. 2019, 5, 1959–1964.
- (6) Sheberla, D.; Bachman, J. C.; Elias, J. S.; Sun, C.-J.; Shao-Horn, Y.; Dincă, M. Conductive MOF Electrodes for Stable Supercapacitors with High Areal Capacitance. *Nat. Mater.* **2017**, *16*, 220–224.
- (7) Nam, K. W.; Park, S. S.; dos Reis, R.; Dravid, V. P.; Kim, H.; Mirkin, C. A.; Stoddart, J. F. Conductive 2D Metal-Organic Framework for High-Performance Cathodes in Aqueous Rechargeable Zinc Batteries. *Nat. Commun.* **2019**, *10*, 4948.
- (8) Liu, J.; Song, X.; Zhang, T.; Liu, S.; Wen, H.; Chen, L. 2D Conductive Metal-Organic Frameworks: An Emerging Platform for Electrochemical Energy Storage. *Angew. Chem., Int. Ed.* **2021**, *133*, 5672–5684.
- (9) Mekata, M. Kagome: The Story of the Basketweave Lattice. *Phys. Today* **2003**, *56*, 12–13.
- (10) Clough, A. J.; Skelton, J. M.; Downes, C. A.; de la Rosa, A. A.; Yoo, J. W.; Walsh, A.; Melot, B. C.; Marinescu, S. C. Metallic Conductivity in a Two-Dimensional Cobalt Dithiolene Metal-Organic Framework. *J. Am. Chem. Soc.* **2017**, *139*, 10863–10867.
- (11) Yoon, S.; Talin, A. A.; Stavila, V.; Mroz, A. M.; Bennett, T. D.; He, Y.; Keen, D. A.; Hendon, C. H.; Allendorf, M. D.; So, M. C. From N- to p-Type Material: Effect of Metal Ion on Charge Transport in Metal-Organic Materials. *ACS Appl. Mater. Interfaces* **2021**, 13, 52055–52062.
- (12) Zhou, Q.; Wang, J.; Chwee, T. S.; Wu, G.; Wang, X.; Ye, Q.; Xu, J.; Yang, S.-W. Topological Insulators Based on 2D Shape-Persistent Organic Ligand Complexes. *Nanoscale* **2015**, *7*, 727–735.

- (13) Sheberla, D.; Sun, L.; Blood-Forsythe, M. A.; Er, S.; Wade, C. R.; Brozek, C. K.; Aspuru-Guzik, A.; Dincă, M. High Electrical Conductivity in Ni₃(2,3,6,7,10,11-Hexaiminotriphenylene)₂, a Semiconducting Metal-Organic Graphene Analogue. *J. Am. Chem. Soc.* **2014**, *136*, 8859–8862.
- (14) Hmadeh, M.; Lu, Z.; Liu, Z.; Gándara, F.; Furukawa, H.; Wan, S.; Augustyn, V.; Chang, R.; Liao, L.; Zhou, F.; Perre, E.; Ozolins, V.; Suenaga, K.; Duan, X.; Dunn, B.; Yamamto, Y.; Terasaki, O.; Yaghi, O. M. New Porous Crystals of Extended Metal-Catecholates. *Chem. Mater.* **2012**, *24*, 3511–3513.
- (15) Eisenberg, R.; Gray, H. B. Noninnocence in Metal Complexes: A Dithiolene Dawn. *Inorg. Chem.* **2011**, *50*, 9741–9751.
- (16) Herebian, D.; Bothe, E.; Neese, F.; Weyhermüller, T.; Wieghardt, K. Molecular and Electronic Structures of Bis-(o-Diiminobenzosemiquinonato)Metal(II) Complexes (Ni, Pd, Pt), Their Monocations and -Anions, and of Dimeric Dications Containing Weak Metal-Metal Bonds. J. Am. Chem. Soc. 2003, 125, 9116–9128.
- (17) Sproules, S.; Wieghardt, K. Dithiolene Radicals: Sulfur K-Edge X-Ray Absorption Spectroscopy and Harry's Intuition. *Coord. Chem. Rev.* **2011**, 255, 837–860.
- (18) Campbell, M. G.; Sheberla, D.; Liu, S. F.; Swager, T. M.; Dincă, M. Cu₃(Hexaiminotriphenylene)₂: An Electrically Conductive 2D Metal-Organic Framework for Chemiresistive Sensing. *Angew. Chem., Int. Ed.* **2015**, *54*, 4349–4352.
- (19) Stanger, A. Nucleus-Independent Chemical Shifts (NICS): Distance Dependence and Revised Criteria for Aromaticity and Antiaromaticity. *J. Org. Chem.* **2006**, *71*, 883–893.
- (20) Mancuso, J. L.; Mroz, A. M.; Le, K. N.; Hendon, C. H. Electronic Structure Modeling of Metal-Organic Frameworks. *Chem. Rev.* **2020**, *120*, 8641–8715.
- (21) Wu, G.; Huang, J.; Zang, Y.; He, J.; Xu, G. Porous Field-Effect Transistors Based on a Semiconductive Metal-Organic Framework. *J. Am. Chem. Soc.* **2017**, *139*, 1360–1363.
- (22) Foster, M. E.; Sohlberg, K.; Allendorf, M. D.; Talin, A. A. Unraveling the Semiconducting/Metallic Discrepancy in Ni₃(HITP)₂. *J. Phys. Chem. Lett.* **2018**, *9*, 481–486.
- (23) Dou, J.-H.; Sun, L.; Ge, Y.; Li, W.; Hendon, C. H.; Li, J.; Gul, S.; Yano, J.; Stach, E. A.; Dincă, M. Signature of Metallic Behavior in the Metal-Organic Frameworks M₃(Hexaiminobenzene)₂ (M = Ni, Cu). *J. Am. Chem. Soc.* **2017**, *139*, 13608–13611.
- (24) Chen, S.; Dai, J.; Zeng, X. C. Metal-Organic Kagome Lattices $M_3(2,3,6,7,10,11$ -Hexaiminotriphenylene)₂(M = Ni and Cu): From Semiconducting to Metallic by Metal Substitution. *Phys. Chem. Chem. Phys.* **2015**, *17*, 5954–5958.
- (25) Tie, D. Y.; Chen, Z. First Principles Study of the Electronic Properties of a Ni₃(2,3,6,7,10,11-Hexaaminotriphenylene)₂ Monolayer under Biaxial Strain. *RSC Adv.* **2015**, *5*, 55186–55190.
- (26) Le, K. N.; Hendon, C. H. Pressure-Induced Metallicity and Piezoreductive Transition of Metal-Centres in Conductive 2-Dimensional Metal-Organic Frameworks. *Phys. Chem. Chem. Phys.* **2019**, 21, 25773–25778.
- (27) Zhao, B.; Zhang, J.; Feng, W.; Yao, Y.; Yang, Z. Quantum Spin Hall and $\rm Z_2$ Metallic States in an Organic Material. *Phys. Rev. B* **2014**, 90, 201403.
- (28) Park, J.; Lee, M.; Feng, D.; Huang, Z.; Hinckley, A. C.; Yakovenko, A.; Zou, X.; Cui, Y.; Bao, Z. Stabilization of Hexaaminobenzene in a 2D Conductive Metal-Organic Framework for High Power Sodium Storage. *J. Am. Chem. Soc.* **2018**, *140*, 10315—10323.
- (29) Choi, J. Y.; Flood, J.; Stodolka, M.; Pham, H. T. B.; Park, J. From 2D to 3D: Postsynthetic Pillar Insertion in Electrically Conductive MOF. ACS Nano 2022, 16, 3145–3151.
- (30) Wang, W.; Zhang, Y.; Chen, L.; Chen, H.; Hu, S.; Li, Q.; Liu, H.; Qiao, S. Tricycloquinazoline-Containing 3D Conjugated Microporous Polymers and 2D Covalent Quinazoline Networks: Microstructure and Conductivity. *Polym. Chem.* **2021**, *12*, 650–659.
- (31) Dou, J.-H.; Arguilla, M. Q.; Luo, Y.; Li, J.; Zhang, W.; Sun, L.; Mancuso, J. L.; Yang, L.; Chen, T.; Parent, L. R.; Skorupskii, G.;

- Libretto, N. J.; Sun, C.; Yang, M. C.; Dip, P. V.; Brignole, E. J.; Miller, J. T.; Kong, J.; Hendon, C. H.; Sun, J.; Dinca, M. Atomically Precise Single-Crystal Structures of Electrically Conducting 2D Metal-Organic Frameworks. *Nat. Mater.* **2021**, *20*, 222–228.
- (32) Sang, M.; Cao, S.; Yi, J.; Huang, J.; Lai, W.-Y.; Huang, W. Multi-Substituted Triazatruxene-Functionalized Pyrene Derivatives as Efficient Organic Laser Gain Media. RSC Adv. 2016, 6, 6266–6275.
- (33) Sadak, A. E.; Karakuş, E.; Chumakov, Y. M.; Dogan, N. A.; Yavuz, C. T. Triazatruxene-Based Ordered Porous Polymer: High Capacity CO₂, CH₄, and H₂ Capture, Heterogeneous Suzuki-Miyaura Catalytic Coupling, and Thermoelectric Properties. *ACS Appl. Energy Mater.* **2020**, 3, 4983–4994.
- (34) Rakstys, K.; Abate, A.; Dar, M. I.; Gao, P.; Jankauskas, V.; Jacopin, G.; Kamarauskas, E.; Kazim, S.; Ahmad, S.; Grätzel, M.; Nazeeruddin, M. K. Triazatruxene-Based Hole Transporting Materials for Highly Efficient Perovskite Solar Cells. *J. Am. Chem. Soc.* **2015**, 137, 16172–16178.
- (35) Gershoni-Poranne, R.; Stanger, A. The NICS- XY -Scan: Identification of Local and Global Ring Currents in Multi-Ring Systems. *Chem. Eur. J.* **2014**, 20, 5673–5688.
- (36) Warren, G. I.; Barker, J. E.; Zakharov, L. N.; Haley, M. M. Enhancing the Antiaromaticity of s-Indacene through Naphthothiophene Fusion. *Org. Lett.* **2021**, 23, 5012–5017.
- (37) Frisch, M. J.; Trucks, G. W.; Schlegel, H. B.; Scuseria, G. E.; Robb, M. A.; Cheeseman, J. R.; Scalmani, G.; Barone, V.; Petersson, G. A.; Nakatsuji, H.; et al. *Gaussian 09, Revision E.01*; Gaussian, Inc.: Wallingford CT, 2016.
- (38) Kresse, G.; Furthmüller, J. Efficient Iterative Schemes for *Ab Initio* Total-Energy Calculations Using a Plane-Wave Basis Set. *Phys. Rev. B* **1996**, *54*, 11169–11186.
- (39) Perdew, J. P.; Ruzsinszky, A.; Csonka, G. I.; Vydrov, O. A.; Scuseria, G. E.; Constantin, L. A.; Zhou, X.; Burke, K. Restoring the Density-Gradient Expansion for Exchange in Solids and Surfaces. *Phys. Rev. Lett.* **2008**, *100*, 136406.
- (40) Schimka, L.; Harl, J.; Kresse, G. Improved Hybrid Functional for Solids: The HSEsol Functional. *J. Chem. Phys.* **2011**, *134*, 024116.